Journal of Nuclear Medicine, published on October 15, 2015 as doi:10.2967/jnumed.115.162990

Motion correction of ^{18}F-sodium fluoride PET for imaging coronary atherosclerotic plaques

Mathieu Rubeaux[1], Nikhil Joshi[2], Marc R. Dweck[2], Alison Fletcher[2], Manish Motwani[1], Louise E. Thomson[1] , Guido Germano[1], Damini Dey[1], Debiao Li[1], Daniel S. Berman[1], David E. Newby[2], Piotr J. Slomka[1]

[1] Cedars-Sinai Medical Center, Los Angeles, CA, USA;

[2] University of Edinburgh, Edinburgh, United Kingdom

Corresponding Author

Piotr J. Slomka, PhD
Artificial Intelligence in Medicine Program
8700 Beverly Blvd, Ste A047N
Los Angeles, CA 90048, USA
piotr.slomka@cshs.org

First Author

Mathieu Rubeaux, PhD
Artificial Intelligence in Medicine Program
8700 Beverly Blvd, Ste A047N
Los Angeles, CA 90048, USA
mathieu.rubeaux@cshs.org

Word Count: 4987

Financial Support: No current conflict of interest related to this work.

Piotr Slomka and Dan Berman receive research grant support from Siemens Medical systems.

Running foot line: Motion corrected ^{18}F-sodium fluoride PET

ABSTRACT

Ruptured coronary atherosclerotic plaques commonly cause acute myocardial infarction. It has been recently shown that active microcalcification in the coronary arteries, one of the features that characterizes vulnerable plaques at risk of rupture, can be imaged using ^{18}F-sodium fluoride (^{18}F-NaF) PET. We aimed to determine whether a motion correction technique applied to gated ^{18}F-NaF PET images could enhance image quality and improve uptake estimates. **Methods:** Seventeen patients with myocardial infarction (n=7) and stable angina (n=10) underwent ^{18}F-NaF PET and prospective coronary CT angiography (CCTA). PET data were reconstructed in 4 different ways: (i) one gated bin (end-diastolic phase with 25% of the counts), (ii) 4 gated bins (consecutive 25% segments), (iii) 10 gated bins (consecutive 10% segments), and (iv) ungated. Subsequently, gated PET images were registered using a local and non-linear motion correction method guided by the extracted coronary arteries from CT angiography using either 4 or 10 bins. Global noise levels and target-to-background ratios (TBR) defined on manually delineated coronary plaque lesions were compared to assess image quality and uptake estimates. **Results:** Compared to the reference standard of using only one bin of PET data, motion correction using the 10 bins of PET data reduced image noise (-46%, $p<0.0001$). TBR in positive lesions was 11% higher using 10-bin motion corrected data, compared to one-bin data (1.98 [IQR 1.70-2.37] *vs* 1.78 [IQR 1.58-2.16], $p=0.0027$), and 33% higher compared to ungated data (1.98 [IQR 1.70-2.37] *vs* 1.48 [IQR 1.39-1.88], $p<0.0001$). **Conclusion:** Motion correction of gated ^{18}F-NaF PET/CCTA is feasible, reduces image noise and increases TBR. This improvement may allow more reliable identification of vulnerable coronary artery plaques using ^{18}F-NaF PET.

Key Words: Motion correction, ^{18}F-sodium fluoride PET imaging, coronary atherosclerotic plaques, microcalcification.

INTRODUCTION

Acute myocardial infarction (AMI) is the leading cause of death with 735,000 Americans experiencing an AMI, and ~120,000 dying as a consequence each year (*1*). AMI most commonly results from coronary atherosclerotic plaque rupture. Despite this, current treatment algorithms make no allowance for the presence or absence of vulnerable plaques at risk of rupture, and the current dogma is to treat all patients with any atherosclerosis in the same way. An accurate, non-invasive a priori method for identifying such rupture-prone plaques would challenge this, allowing high-risk patients to be selectively targeted with patient-specific therapies.

Histopathological studies of patients who died from AMI have demonstrated that the plaques that have ruptured and caused AMI have several common characteristics. Among these features, microcalcification is a consistent finding, believed to represent the very early stages of the body's attempts to heal inflamed necrotic plaque. In a recent series of studies (*2-4*), it has been demonstrated that positron emission tomography (PET) imaging with ^{18}F-sodium fluoride (^{18}F-NaF) – an inexpensive, FDA-approved, and widely available tracer–binds preferentially to regions of vascular microcalcification and that it can be used to identify high-risk plaques and plaque rupture in the coronary arteries. In particular, Joshi et al have demonstrated that increased ^{18}F-NaF PET activity localized to exact site of plaque rupture in >90% of patients who had recently suffered AMI, independent of stenting (*2*).

There are, however, still a number of important limitations to be addressed. The difference in target-to-background ratio (TBR) between culprit (implicated in AMI) and non-culprit plaques in ^{18}F-NaF PET is relatively small (~34%), due to blurring of coronary uptake by cardiac, respiratory, and patient motion. The implication is a greater risk of misclassification when this

technique is applied to real-world, unselected populations. Unfortunately, recent general purpose motion correction methods proposed for PET (*5*,*6*) are not applicable, due to lack of clear anatomical landmarks in the heart region on the ^{18}F-NaF scan. To partially address the problem of motion, only one cardiac phase (representing about ¼ of the PET data) was used in the initial study (*2*), at the expense of significant noise increase. Although this was a useful exploratory strategy, the combination of an already narrow diagnostic TBR margin with increased noise is clearly suboptimal.

We have previously developed motion correction techniques for cardiac perfusion data from SPECT and PET, which facilitated an increase in image contrast compared to ungated data (*7*,*8*). In the present study, we aim to overcome some of the current limitations of ^{18}F-NaF PET, by developing a new motion correction method for coronary ^{18}F-NaF PET in order to optimize this promising plaque imaging technique.

MATERIALS AND METHODS

Patients

Patients were recruited from the Royal Infirmary of Edinburgh between February, 2012, and January, 2013, in two cohorts: 7 patients with acute ST-segment or non ST-segment elevation AMI and 10 patients with stable angina pectoris undergoing elective invasive coronary angiography. Table 1 shows the demographic and clinical characteristics of these patients. All patients underwent a comprehensive baseline clinical assessment, including evaluation of their cardiovascular risk factor profile. Studies were done with the approval of the local research ethics committee, in accordance with the Declaration of Helsinki, and with the written informed consent of each participant.

Imaging and Analysis Protocols

All patients underwent cardiac-gated ^{18}F-NaF PET/CT imaging of the coronary arteries with a hybrid scanner (64-multidetector Biograph mCT, Siemens Medical Systems, Erlangen, Germany). Study subjects were administered a target dose of 125 MBq ^{18}F-NaF intravenously, and subsequently rested in a quiet environment for 60 min. An attenuation correction CT scan (non-enhanced 120 kV and 50 mA) was then performed, followed by PET imaging of the thorax in list-mode for 20 min.

Prospectively-gated coronary CT angiography (CCTA) was undertaken in the same visit as the ^{18}F-NaF scan a. CCTA was performed using the following settings: 330 ms rotation time, 100 (body mass index [BMI] <25 kg/m^2) or 120 (BMI >25 kg/m^2) kV tube voltage, 160-245 mAs tube current, 3.8 mm/rotation table feed, with prospective ECG-triggering (heart rate regular and <60beats/min), or retrospective (heart rate >60 beats/min) ECG-gating. Depending on the BMI, a bolus of 80-100 mL of contrast (400 mgI/mL; Iomeron, Bracco, Milan, Italy) was injected intravenously at 5 mL/s, after determining the appropriate trigger delay with a test bolus of 20 mL contrast material. ECG-gated PET images were reconstructed using the Siemens Ultra-HD (time-of-flight plus point spread function) algorithm in multiple phases of the cardiac cycle. For this study, 4 different sets of data were reconstructed from list mode data: one bin with 25% of the counts during the end-diastolic phase –technique used in the original Joshi et al study (*2*), 4 bins, 10 bins, and ungated. The PET pixel size was 2 mm. The CCTA scans were reconstructed at 0.75 x 0.7 mm and 0.6 x 0.3 mm for retrospective and prospective acquisitions respectively at 70% of the cardiac cycle.

Motion Correction

The goal of the motion correction procedure was to compensate for coronary artery motion in the different phases of the ECG-gated PET data. Gated PET with 4 and 10 time bins were reconstructed from the PET list-mode files. The registration aimed to align all bins to the end-diastolic phase position, synchronizing the registered data to i) the prospective CCTA and ii) the one bin PET data corresponding to the end-diastolic phase (as used in the original study), for comparison purposes. The end-diastolic phase, taken as the reference, corresponded to bin 3 in the dataset with 4 bins, and to bin 7 in the dataset with 10 bins.

The registration of individual bins of ^{18}F-NaF PET presents a unique challenge, since there are no clear anatomical references in the heart's vicinity, and bone motion (where there is significant ^{18}F-NaF uptake) is not correlated with coronary motion. Thus, innovative approaches are required to deal with this problem. The procedure we used is illustrated in Figure 1. In order to recover the anatomical information that is missing in the PET data, we used the CCTA data that clearly delineates the coronary arteries. End-expiration position of the CCTA allowed very good alignment with PET data when patient remains in the same position. Coronary regions were first extracted from the CCTA by vessel tracking based on Bayesian maximal paths (*9*), as implemented and validated in our Autoplaq CCTA processing software (*10-12*). This algorithm only requires proximal and distal points for every coronary artery as input, and automatically finds the vessel centerline. The centerlines of the right coronary artery (RCA), left circumflex artery (LCX) and left anterior descending (LAD) coronary artery were extracted for every patient in this manner.

Subsequently, the centerline coordinates were transferred to the PET volumes to automatically extract 3D tubular volumes of interest (VOI) surrounding the coronary arteries in

the gated PET images, defined by a 20-mm radius around each centerline. This radius was chosen to take into account the maximum displacement that can occur during the cardiac cycle, also allowing for potential remaining misregistration. Techniques that did not constrain the registration by coronary vessel regions were hampered by noise adjacent to the coronary arteries.

Next, a non-linear level-set algorithm (*13*) was applied to the extracted coronary regions and constrained according to the expected coronary artery motion. Every VOI of the PET data from each bin was then registered to the end-diastolic reference artery region. The advantage of this method as compared to other non-linear registration techniques is the computational efficiency and knowledge-based estimation of the expected arterial motion. After the registration process, all the registered VOIs were inserted back in their original PET image, using a linear gradient at the border between the registered VOI and the non-registered original PET image to blend both volumes and ensure smooth transition between both regions. Finally, all registered PET images were summed into one volume. In this manner, we obtained static 4-bin and 10-bin motion corrected PET data.

Lesion and Target-to-Background Ratio

To define the lesions, PET data were fused with the CCTA, and analyzed by experienced observers blinded to the clinical diagnosis (NJ, MD) using an OsiriX workstation (OsiriX Imaging Software, Geneva, Switzerland). Two dimensional regions of interest were drawn around all major (diameter >2 mm) epicardial vessels on 3-mm axial slices just beyond the discernible adventitial border. We used a previously established 95% lower reference limit to categorize coronary plaques into ^{18}F-NaF positive and negative lesions, on the end-diastolic data as in the original study. Focal uptake with a target to background (TBR) more than 25% higher than a proximal reference lesion were categorized as ^{18}F-NaF positive plaques, or as negative

plaques if these criteria were not achieved. This limit was based on our previous study, where plaques with high ^{18}F-NaF uptake had maximum TBRs that were 44% (95% CI 26–62) higher than a proximal quiescent reference lesion.(*3*)

TBR measurements were defined as the ratio between the maximum activity values in the manually defined lesion over the mean value of the background, taken to be the blood pool in the middle of the left ventricle. This region was positioned to include the whole blood pool region in mid-ventricular slice for each patient. The noise was determined as the ratio of the mean over the standard deviation of the background.

Statistical Analysis

Statistical analyses were performed with Analyse-it software (Analyse-it, Leeds, UK). For all continuous variables, the Shapiro-Wilk test was used to assess normality. All continuous variables were described as mean ± standard deviation or median and interquartile range (IQR). Non-parametric results were presented as median (IQR) and compared using the Wilcoxon signed-rank test as appropriate. A two-sided $p<0.05$ was taken as statistically significant.

RESULTS

Patients were predominantly middle-aged men and had multiple cardiovascular risk factors (Table 1). Radiation exposure for CCTA and PET is summarized in Table 2. The algorithm successfully registered the gated data for all studies, as assessed visually in the cinematic display. The approximate processing time was about 1 min/study. The results were computed and compared for the 4 sets of reconstructed data: one single PET bin corresponding to the end-diastolic phase, as presented in the initial trial (*2*), 4 and 10 bins that were motion corrected as

described above, and ungated data. In total, 51 lesions (28 positive, 23 negative) were delineated in the 17 patients. These lesions were distributed over the major coronary arteries: 17 (33%) in the LAD, 21 (41%) in the RCA and 13 (26%) in the LCX. TBR ratio in positive and negative lesions was measured in the 4 sets of data presented above.

Activity

^{18}F-NaF activity (expressed as TBR) in the positive lesions with the 10-bin motion corrected data was 11% higher as compared to one-bin data (1.98 [IQR 1.70-2.37] *vs* 1.78 [IQR 1.58-2.16], p=0.0027), and 33% higher as compared to ungated data (1.98 [IQR 1.70-2.37] *vs* 1.48 [IQR 1.39-1.88], p<0.0001). In contrast, no difference was observed when comparing one- to 4-bin motion corrected data (1.78 [IQR 1.58-2.16] *vs* 1.75 [IQR 1.50-2.16], p=0.77). (Figure 2A)

In ^{18}F-NaF negative lesions, we observed some differences between one- and 4-bin motion corrected data (0.90 [IQR 0.70-1.05] *vs* 0.91 [IQR 0.76-1.09], p=0.006) as well as between one- and 10-bin motion corrected data (0.90 [IQR 0.70-1.05] *vs* 0.93 [IQR 0.80-1.04], p=0.025), (Figure 2B) but these absolute differences were much smaller than for the ^{18}F-NaF positive lesions. Furthermore, the median TBR in the ^{18}F-NaF negative lesions were all < 1.0 for all techniques.

Overall, the median TBR difference between ^{18}F-NaF positive and negative lesions increased from 0.88 to 1.05 using the 10-bin motion corrected data, as compared to one bin. This technique should therefore allow for a better discrimination between positive and negative lesions, as compared to the single end-diastolic bin alone that was presented in the original trial (*2*).

Noise

Noise was significantly reduced by using the 4- or 10-bin motion correction method as compared to the single end-diastolic bin: 0.09 [IQR 0.08-0.12] *vs* 0.18 [IQR 0.15-0.24], p<0.0001 (Figure 2C). This is an expected finding since only a quarter of the PET counts were used in the one bin data. Noise was essentially the same for ungated data and motion corrected 4-bin and 10-bin data, since all the PET counts were used by all of these 3 techniques.

Image examples illustrating noise decrease and TBR improvements are shown in Figures 3, 4 and 5.

Motion

We also computed the maximal motion of the coronary plaques that occurred in the different arteries during the motion correction process. The median end-systolic to end-diastolic displacement was 17.2 mm [IQR 14.6-19.0 mm] in the LAD, 17.7 mm [IQR 16.1-20.7 mm] in the LCX, and 19.4 mm [IQR 16.2-22 mm] in the RCA. These results are in accordance with the range of the coronary motion during the cardiac cycle that has been reported in the literature (*14*).

DISCUSSION

We have developed a new motion correction method to tackle coronary motion in ^{18}F-NaF PET imaging data by applying level-set based non-linear PET registration of individual PET time-bins to the end-diastolic position. This registration was constrained to the coronary regions extracted from the co-registered CCTA to avoid registration to spurious noise signal outside of the coronary regions. As compared to the original method (*2*), we have demonstrated increased

TBRs, while drastically reducing noise (Figure 4). The best results are obtained for the 10-bin motion corrected data since it provides the best time-resolved motion correction.

Previous studies have addressed cardiac motion correction in PET and SPECT (*7,8*). Dual-gating (cardiac/respiratory) (*15,16*) and dual-correction have been reported by several groups (*5, 6,17,18*). However, all of these methods depend on the uptake in anatomical organs, (in case of cardiac imaging—the myocardium) and therefore are not applicable to coronary PET. ^{18}F-NaF PET represents a unique challenge, since there are no clear anatomical references in the heart's vicinity, and bone motion (where there is significant ^{18}F-NaF uptake) is not correlated with coronary motion. To our knowledge, this is the first report of motion corrected coronary PET by the use of such non-linear registration methods.

Our technical development study also has several important implications for the future of coronary ^{18}F-NaF PET imaging, which in its infancy has been hampered by cardiac motion, radiation exposure and cost. The initial approach to motion was to discard all the PET counts when the heart was moving resulting in high noise in the end-diastolic PET data. This might ultimately limit the accuracy and clinical utility of ^{18}F-NaF PET in distinguishing true uptake in culprit/high-risk sites from noise-related false-positives. The improved separation of positive and negative lesions and noise reduction enabled by this motion correction method will likely enhance the capability of ^{18}F-NaF PET and lead to more optimal detection of vulnerable plaques. Our technique retains the count statistics from the full PET acquisition and at the same time increases the TBR as compared to the original one-bin method. This ultimately may facilitate

reduced bed times (improving scan efficiency and reducing costs) or reduced tracer dose/radiation exposure.

In this study, CCTA scans were obtained in the original clinical protocol for the purposes of PET uptake localization and plaque characterization. We opted to use these scans as the anatomical framework for PET motion correction since the data were readily available. To our knowledge, all coronary PET studies (with ^{18}F-NaF or ^{18}F-FDG) to date have utilized contrast CCTA for localization of PET uptake (*2,19,20*). Other registration methods which do not utilize CCTA could be explored in the future such as with the PET/MR systems. Alternatively, ^{18}F-NaF PET testing could be applied in patients who have already undergone prior anatomical testing with CCTA and present abnormal results with potentially vulnerable plaques. Under such circumstances, the prior CCTA could be re-used (after co-registration to the PET scan or CT attenuation scan obtained with ^{18}F-NaF PET) to localize the ^{18}F-NaF PET uptake and guide the motion correction without adding additional radiation or contrast exposure. Furthermore, we have used the method of Vemuri et al. (*13*) for the non-linear registration of the multiple bins of PET data in the selected coronary regions. This method is computationally efficient, which is important since multiple volume registrations are required for each patient. Other registration algorithms, such as the latest optical flow methods, may have additional benefits that warrant further exploration. Given our demonstration of the feasibility of a nonlinear motion correction method for improved coronary PET imaging, these other approaches and refinements warrant further prospective investigation and validation in future studies.

The incorporation of the CCTA's anatomical framework as proposed here, can also potentially lead to automation and reproducibility of quantitative analysis of PET uptake, allowing less experienced centers to immediately implement this technique and fostering meaningful inter-center comparisons of the data. It is of key importance that this promising new PET technique is allowed to reach its full potential by optimizing the image analysis techniques. The new CCTA-guided motion correction technique as proposed in this work will be also applicable to future PET tracers exploring the pathological processes in the coronary vasculature.

For patients with coronary heart disease, ^{18}F-NaF PET technique has a number of applications. First, it may help assess future risk and provide added value to the simple anatomical assessment from CCTA. This may help inform the intensity of medical therapy as well as plan potential coronary revascularization, especially for intermediate lesions or those with multivessel disease. It may also help determine risk in the context of non-cardiac interventions, such as the planning of non-cardiac surgery. Finally, it may also provide a surrogate biomarker of plaque vulnerability against which novel therapeutic interventions can be assessed.

This study has several limitations. While it clearly shows significant gains in image quality by the motion correction method applied to ^{18}F-NaF PET imaging, there is room for further improvement. Indeed, we are likely to achieve further significant enhancements in TBR by incorporating respiratory and patient motion correction, as well as correction for partial volume effects. We have not performed these additional corrections in our study since the dual gating and combined correction for these additional motions is a complex problem. Potentially, PET

and CCTA may be misregistered even if CCTA is acquired in end-expiration. Therefore, the CCTA coronary regions may not be exactly corresponding to the PET regions considered in the motion correction technique. Correcting for this alignment automatically may result in possible further improvements, since our method relies on centerlines extraction from the CCTA, which define 3D regions-of-interest in PET data. Nevertheless, the regions used were encompassing an approximate coronary artery path of 2 cm diameter, which should allow for some CCTA-PET misregistration. We did not use standard uptake values (SUV) in this study, focusing instead on TBR. In our experience, SUV data results in greater variability than the TBR values, although this may need to be reevaluated when partial volume corrections are performed. We acknowledge that this study cohort is small, reflecting the novelty of coronary imaging by ^{18}F-NaF PET. Nevertheless, since there were multiple lesions in each patient, we were able to demonstrate the significant improvements afforded by our technique. In this study we focus on improvement in image quality and discrimination of ^{18}F-NaF PET positive and negative lesions, rather than the clinical utility of coronary ^{18}F-NaF PET. An ongoing prospective study (NCT02278211) aims to demonstrate the value of coronary ^{18}F-NaF PET technique in prediction of future myocardial infarction (*21*). We plan to apply the developed techniques to demonstrate improved prediction of myocardial infarction when this trial is completed.

CONCLUSION

Motion correction of gated ^{18}F-NaF PET/CT reduces noise and increases target-to-background ratio as compared to one-bin imaging and further improves target-to-background ratio as compared to ungated images without noise increase. This improvement may allow more reliable identification of vulnerable plaque lesions in the coronary arteries by ^{18}F-NaF PET.

DISCLOSURE

No current conflict of interest related to this work.

Piotr Slomka and Daniel Berman receive research grant support from Siemens Medical systems.

ACKNOWLEDGMENTS

The study was funded by the Chief Scientist Office, Scotland (ETM/160). DN (CH/09/002) and MRD (FS/14/78) are supported by the British Heart Foundation. David Newby is the recipient of a Wellcome Trust Senior Investigator Award (WT103782AIA). The study was also in part supported by a grant (*Cardiac Imaging Research Initiative*) from the Adelson Medical Research Foundation at Cedars-Sinai.

REFERENCES

1. Mozaffarian D, Benjamin EJ, Go AS, et al. Heart disease and stroke statistics--2015 update: a report from the american heart association. *Circulation.* 2015;131:e29-e322.

2. Joshi NV, Vesey AT, Williams MC, et al. 18F-fluoride positron emission tomography for identification of ruptured and high-risk coronary atherosclerotic plaques: a prospective clinical trial. *Lancet.* 2014;383:705-713.

3. Dweck MR, Chow MW, Joshi NV, et al. Coronary arterial 18F-sodium fluoride uptake: a novel marker of plaque biology. *Journal of the American College of Cardiology.* 2012;59:1539-1548.

4. Irkle A, Vesey A, Lewis D, et al. Identifying active vascular microcalcification by 18F-sodium fluoride positron emission tomography. *Nature Communications.* 2015; (in press).

5. Gigengack F, Ruthotto L, Burger M, Wolters CH, Jiang X, Schafers KP. Motion correction in dual gated cardiac PET using mass-preserving image registration. *IEEE Trans Med Imaging.* 2012;31:698-712.

6. Lamare F, Le Maitre A, Dawood M, et al. Evaluation of respiratory and cardiac motion correction schemes in dual gated PET/CT cardiac imaging. *Medical physics.* 2014;41:072504.

7. Slomka PJ, Nishina H, Berman DS, et al. "Motion-frozen" display and quantification of myocardial perfusion. *J Nucl Med.* 2004;45:1128-1134.

8. Le Meunier L, Slomka PJ, Dey D, et al. Motion frozen (18)F-FDG cardiac PET. *Journal of Nuclear Cardiology.* 2011;18:259-266.

9. Lesage D, Angelini ED, Bloch I, Funka-Lea G. Bayesian maximal paths for coronary artery segmentation from 3D CT angiograms. *Med Image Comput Comput Assist Interv.* 2009;12:222-229.

10. Schuhbaeck A, Dey D, Otaki Y, et al. Interscan reproducibility of quantitative coronary plaque volume and composition from CT coronary angiography using an automated method. *Eur Radiol.* 2014;24:2300-2308.

11. Dey D, Achenbach S, Schuhbaeck A, et al. Comparison of quantitative atherosclerotic plaque burden from coronary CT angiography in patients with first acute coronary syndrome and stable coronary artery disease. *J Cardiovasc Comput Tomogr.* 2014;8:368-374.

12. Diaz-Zamudio M, Dey D, Schuhbaeck A, et al. Automated quantitative plaque burden from coronary CT angiography noninvasively predicts hemodynamic significance by using fractional flow reserve in intermediate coronary lesions. *Radiology.* 2015;276:408-415.

13. Vemuri BC, Ye J, Chen Y, Leonard CM. Image registration via level-set motion: applications to atlas-based segmentation. *Medical image analysis.* 2003;7:1-20.

14. Shechter G, Resar JR, McVeigh ER. Displacement and velocity of the coronary arteries: cardiac and respiratory motion. *IEEE Trans Med Imaging.* 2006;25:369-375.

15. Martinez-Moller A, Souvatzoglou M, Navab N, Schwaiger M, Nekolla SG. Artifacts from misaligned CT in cardiac perfusion PET/CT studies: frequency, effects, and potential solutions. *J Nucl Med.* 2007;48:188-193.

16. Koivumaki T, Nekolla SG, Furst S, et al. An integrated bioimpedance--ECG gating technique for respiratory and cardiac motion compensation in cardiac PET. *Phys Med Biol.* 2014;59:6373-6385.

17. Hong I, Jones J, Casey M. Elastic motion correction for cardiac PET studies. *Nuclear Science Symposium and Medical Imaging Conference (NSS/MIC)*, 2013:1-3.

18. Slomka PJ, Rubeaux M, Le Meunier L, et al. Dual-gated motion-frozen cardiac PET with flurpiridaz F18. *J Nucl Med.* 2015;(in press).

19. Cheng VY, Slomka PJ, Le Meunier L, et al. Coronary arterial 18F-FDG uptake by fusion of PET and coronary CT angiography at sites of percutaneous stenting for acute myocardial infarction and stable coronary artery disease. *J Nucl Med.* 2012;53:575-583.

20. Rogers IS, Nasir K, Figueroa AL, et al. Feasibility of FDG imaging of the coronary arteries: comparison between acute coronary syndrome and stable angina. *JACC Cardiovasc Imaging.* 2010;3:388-397.

21. Newby DE, Dweck M. Prediction of recurrent events with 18F-fluoride (PREFFIR). https://clinicaltrials.gov/ct2/show/NCT02278211.

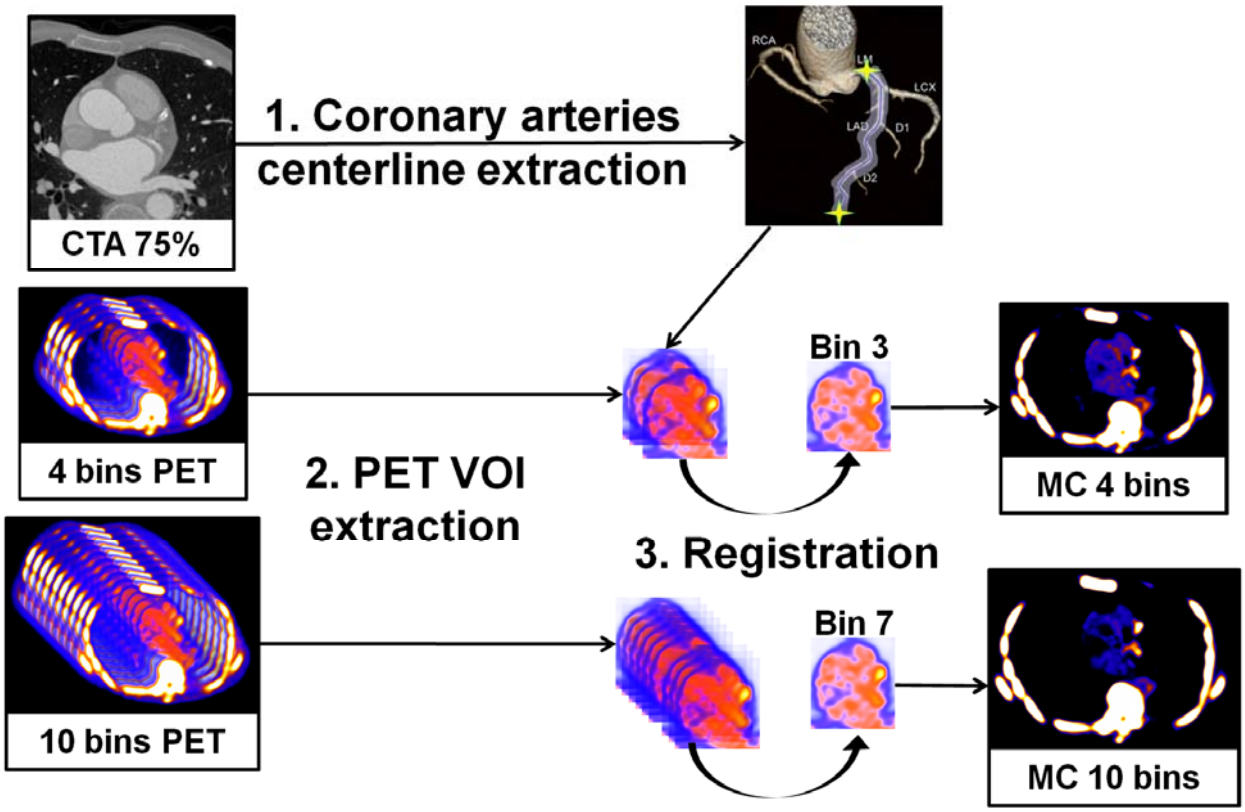

Figure 1. Overview of the motion correction method. 1. Coronary arteries centerlines are extracted from the CCTA in end-diastolic phase using CCTA analysis software. 2. Volumes of interest (VOI) surrounding the coronary arteries are extracted from the 4-bin and 10-bin PET data using the previously extracted CCTA centerlines. 3. All bins of the PET data are registered to the common end-diastolic reference bin (bin 3 and 7 for the 4- and 10-bin data, respectively) by non-linear level-set registration restricted to coronary regions. Then the registered VOIs are inserted back into their original PET volumes, and all registered PET images are summed into one volume to obtain the motion corrected (MC) 4- and 10-bin data.

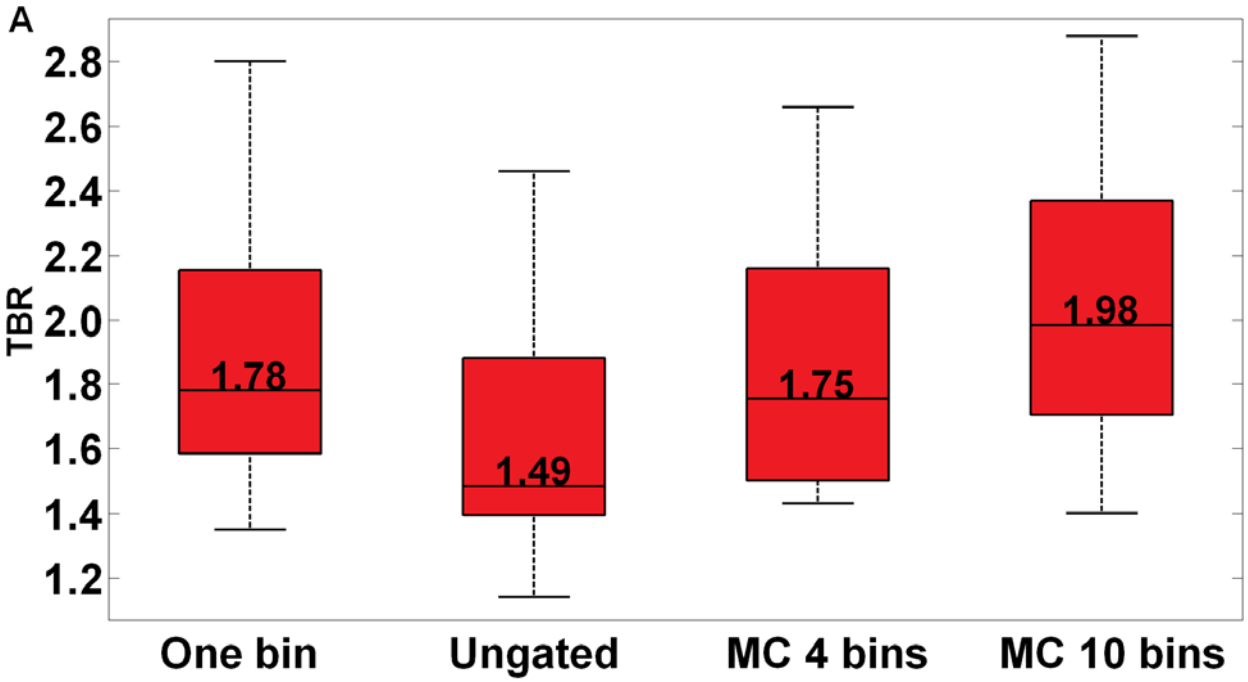
A
TBR
2.8
2.6
2.4
2.2
2.0
1.8
1.6
1.4
1.2
1.78
1.49
1.75
1.98
One bin
Ungated
MC 4 bins
MC 10 bins

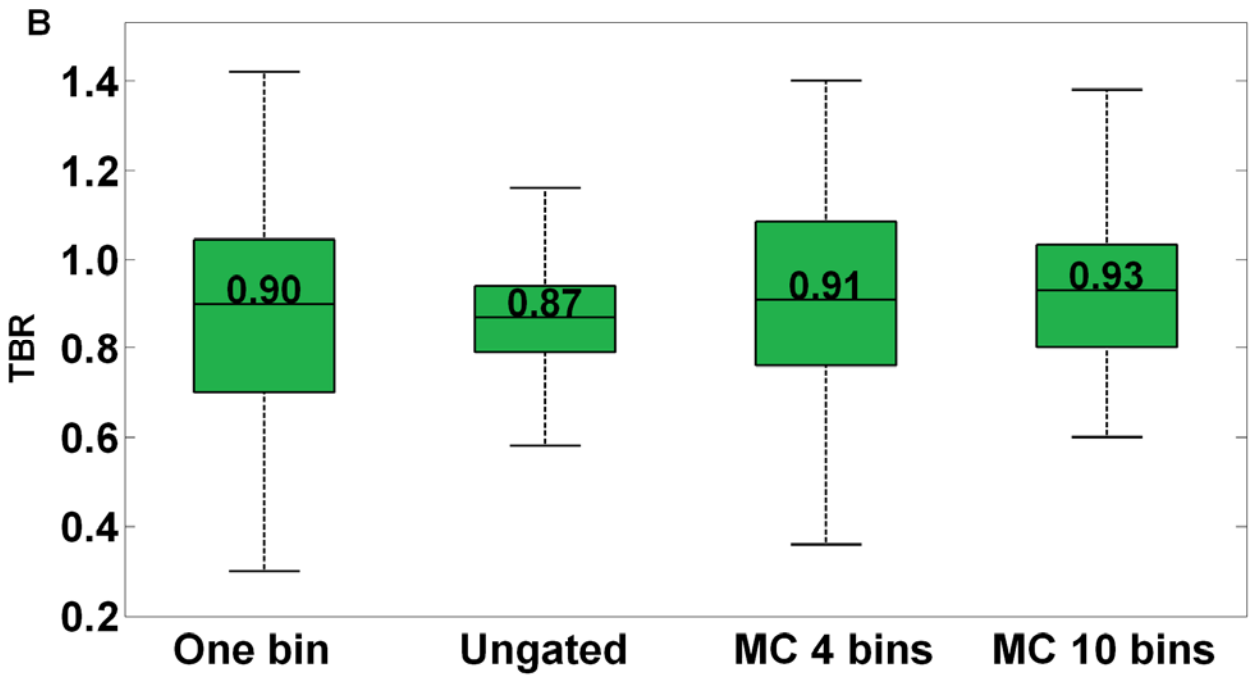
B
TBR
1.4
1.2
1.0
0.8
0.6
0.4
0.2
0.90
0.87
0.91
0.93
One bin
Ungated
MC 4 bins
MC 10 bins

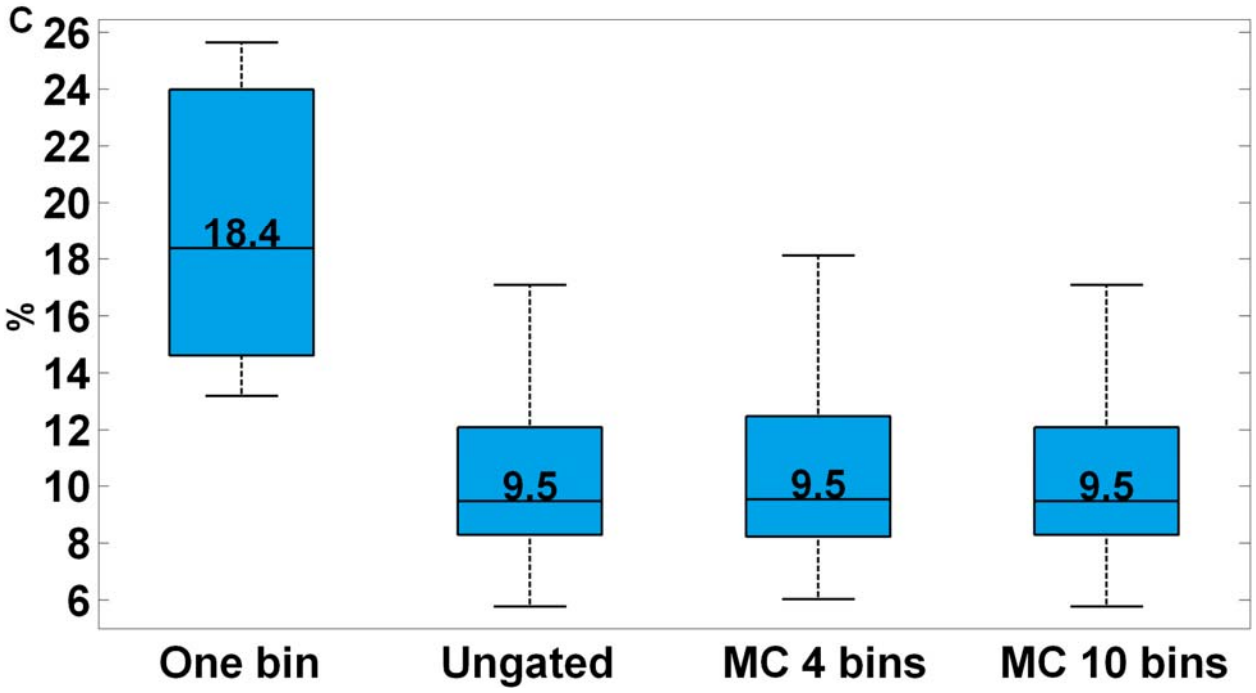

Figure 2. Target-to-background (TBR) ratios in positive (A) and negative (B) lesions and noise (C) is shown for the different datasets (one end-diastolic bin, ungated data, motion corrected (MC) image created from 4 bins and motion corrected image created from 10 bins). A. The TBR in positive lesions increases with motion correction technique with 10-bin data, as compared to one-bin images and to ungated data. B. The TBR in negative lesions remains below 1 using motion correction technique. C. The noise is almost halved using motion correction technique, as compared to the original one-bin data.

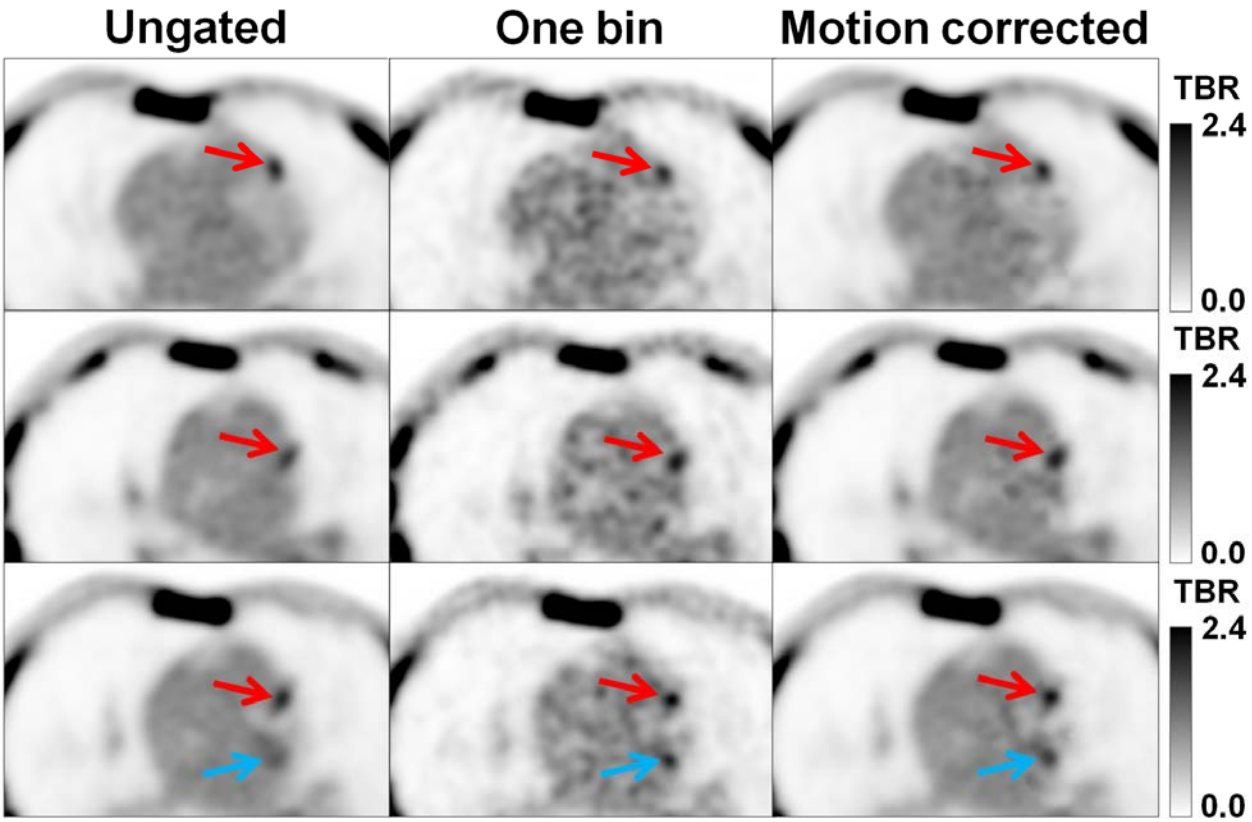

Figure 3. Left anterior descending (LAD) coronary artery (red arrow) and left circumflex (LCX) artery (blue arrow) vulnerable plaques of a 65 year old man using standard linear grayscale display and transaxial slices. The images show blurred lesion signal in ungated image (first column), significant noise in one bin images and high lesion signal with reduced noise in the 10-bin motion corrected image (third column).

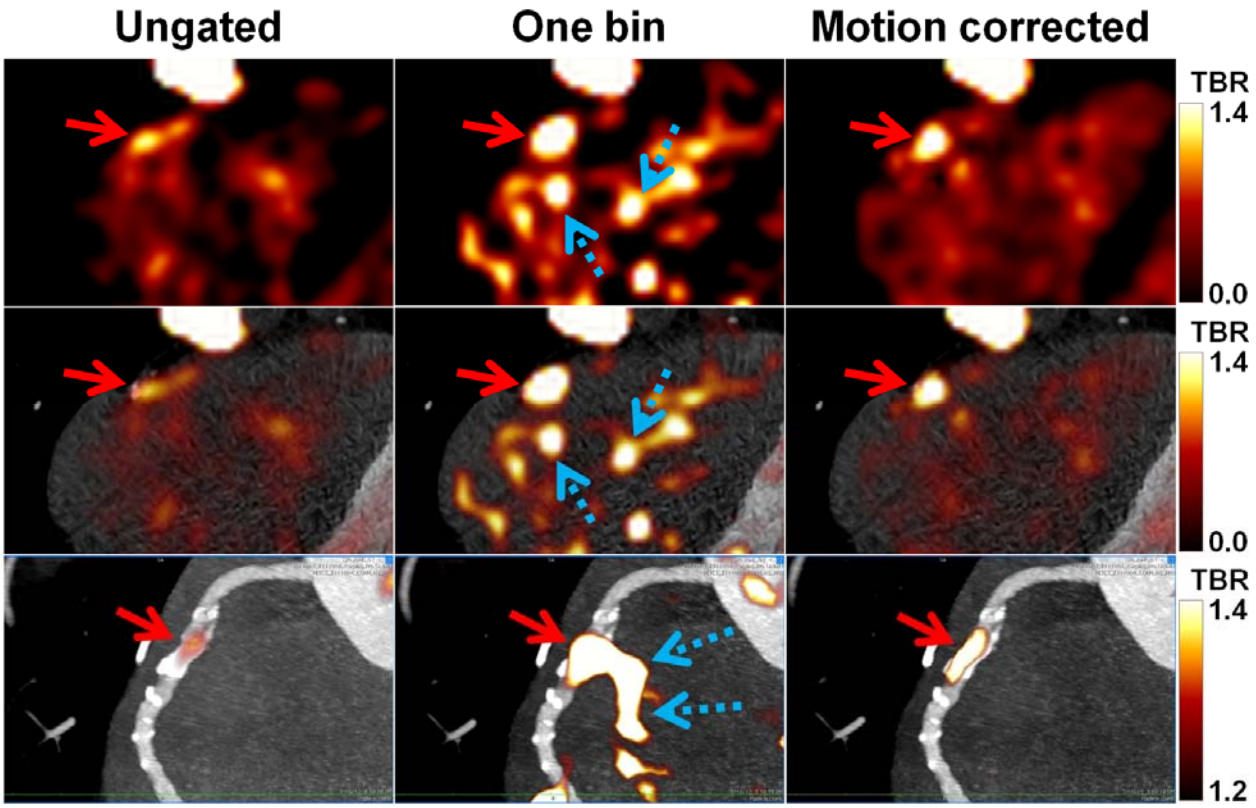

Figure 4. Right coronary artery (RCA) vulnerable plaque, for the same case as in Figure 3. PET images (top row), Fused PET and CCTA (middle row) and multiplanar-reformatted views PET/CCTA (bottom row) of the RCA lesion (red arrows) with exponential color table. The images show the low lesion signal in ungated image (first column), significant noise in one-bin images (blue arrows, second column) and high lesion signal with reduced noise in the 10-bin motion corrected image (third column). Respective ungated, one bin, and motion corrected images were obtained with the same window and level settings.

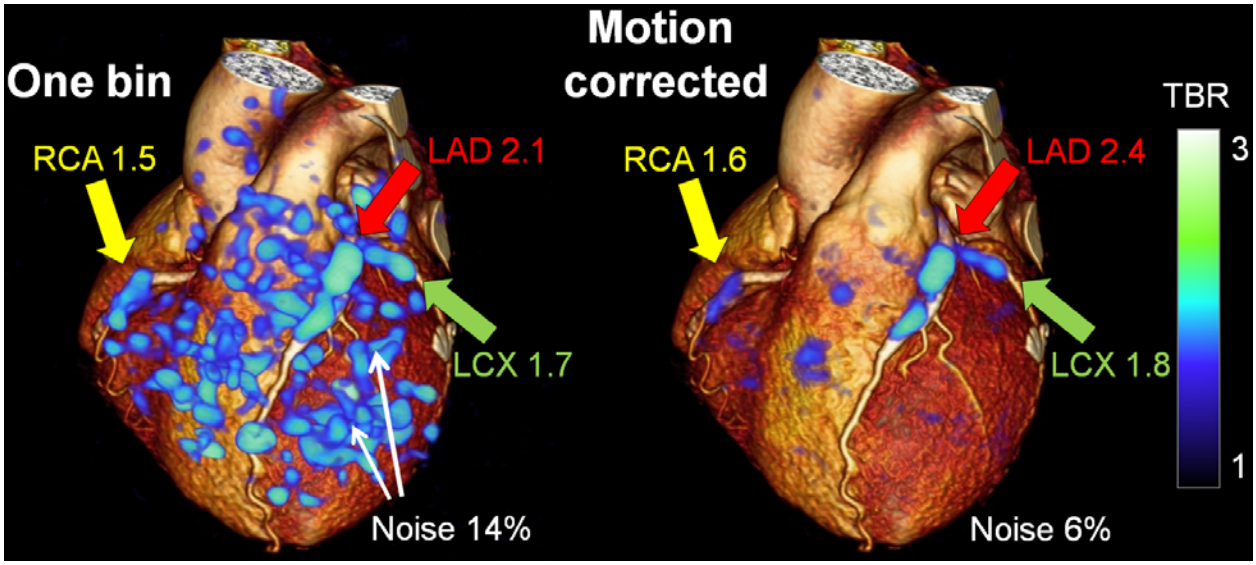

Figure 5. 3D rendering of one-bin PET image (¼ of PET counts) as used in the original study by Joshi et al (left) and new motion corrected PET image (right), superimposed on the rendered CCTA volume, for the same case as in Figure 3 and 4. High noise is seen in one bin image (white arrows). Increased ^{18}F-NaF uptake (broad arrows) is seen in the right coronary artery (RCA; yellow), left anterior descending (LAD; red) coronary artery and left circumflex artery (LCX; green), and remains clearly seen on the motion corrected images without the noise.

TABLE 1

Patient demographic and clinical characteristics

	Stable angina (n=10)	Myocardial infarction (n=7)
Age in years, mean (SD)	67 (9)	66 (7)
Men, n (%)	9 (90%)	7 (100%)
Body-mass index (kg/m^2), mean (SD)	29 (5)	28 (8)
Calcium score (Agatston units), median (IQR)	1010 (560-2175)	498 (355-771)
Cardiovascular history, n (%)		
Previous MI	4 (40%)	0
Previous PCI	5 (50%)	1 (14%)
Previous CABG	5 (50%)	0
Lesions, n (%)	31 (61%)	20 (39%)
Positive	19 (68%)	9 (32%)
Negative	12 (52%)	11 (48%)

MI=myocardial infarction.

PCI=percutaneous coronary intervention. CABG=coronary artery bypass graft

TABLE 2

Patients' radiation exposure in mSv during the study

		^{18}F-NaF	CCTA Dose	AC CT Dose	PET/CT + CCTA
Prospective	**Range (Min-Max)**	**2.8 - 3.1**	**1.3 - 5.8**	**0.5 - 1.8**	**4.7 - 9.9**
	Mean ± SD	**2.9 ± 0.1**	**3.4 ± 1.2**	**1.0 ± 0.4**	**7.3 ± 1.4**
Retrospective	**Range (Min-Max)**	**2.8 - 3.0**	**7.8 - 12.7**	**0.9 - 1.1**	**11.6 - 16.7**
	Mean ± SD	**2.9 ± 0.1**	**9.7 ± 2.7**	**1.0 ± 0.1**	**13.6 ± 2.7**

Conversion factor of 0·014 mSv/mGy.cm for CCTA and AC CT

Conversion factor of 0·024 mSv/MBq for ^{18}F-NaF